International Journal of Pharmaceutics 375 (2009) 97–106

Contents lists available at ScienceDirect

International Journal of Pharmaceutics

journal homepage: www.elsevier.com/locate/ijpharm

Pharmaceutical Nanotechnology

The potential of glycol chitosan nanoparticles as carrier for low water soluble drugs

Adriana Trapani[a,*], Johannes Sitterberg[b], Udo Bakowsky[b], Thomas Kissel[b]

[a] Facoltà di Farmacia, Dipartimento Farmaco-Chimico, Università degli Studi di Bari, via Orabona 4, 70125 Bari, Italy
[b] Department of Pharmaceutics and Biopharmacy, Philipps-University, Ketzerbach 63, D-35032 Marburg, Germany

ARTICLE INFO

Article history:
Received 25 November 2008
Received in revised form 17 March 2009
Accepted 23 March 2009
Available online 11 April 2009

Keywords:
Coumarin
Glycol chitosan
Cyclodextrins
Nanoparticles

ABSTRACT

The laser dye 6-coumarin was selected as model of low water soluble drug to be encapsulated in glycol chitosan nanoparticles intended for transmucosal applications and, at the same time, being a fluorescent probe, it is of aid to elucidate the intracellular fate of the particles. To increase the aqueous solubility of the tracer, the complexation with different cyclodextrins was adopted. The fluorescence properties of the inclusion complexes were evaluated. The increase in aqueous solubility provided by different cyclodextrins [up to 1.4×10^{-4} M in the case of heptakis (2,6-di-O-methyl)-β-cyclodextrin] allowed the preparation of novel glycol chitosan nanoparticles according to the ionic cross-linking of the polycation by sodium tripolyphosphate. Small changes in the preparation technique allowed to produce particles of two different sizes, around 200 nm and bigger than 300 nm where the contribution of cyclodextrin consisted of the modulation encapsulation efficiency in the final particles. Confocal laser scanning microphotographs clearly showed the internalization of 6-coumarin nanoparticles in Caco-2 cell line. The results reveal that these biodegradable nanoparticles hold promise as probes in biomedical field.

1. Introduction

In recent years, chitosan nanoparticles (NPs) have been intensively investigated for drug administration because of the favorable features of the polymer in terms of biocompatibility, non-toxicity and bioadhesion (Mei et al., 2008). The core of such NPs has shown good capability to encapsulate different therapeutics whereas the surface composition of the resulting NPs could be conveniently adapted for targeting purposes. In this regard, the incorporation of cyclodextrins (CDs) in chitosan NPs provided a promising drug carrier system where the benefits of the polysaccharide were combined with the stabilizing role exerted by CDs (Krauland and Alonso, 2007; Trapani et al., 2008). Thus, NPs made of chitosan and hydroxypropyl-β-CD were successfully employed for the administration of lipophilic drugs (Maestrelli et al., 2006). However, chitosan is normally insoluble in solutions above pH 6 and requires acid to be protonated. Therefore, various chemical modifications have been introduced to increase the water solubility of chitosan. Glycol chitosan (GCS, Fig. 1) is a chitosan derivative conjugated with ethylene glycol branches, water soluble at a neutral/acidic pH values where the pendant glycol branches on the polymer increase both the aqueous solubility of the native chitosan and provide steric stabilization. Based on the above-mentioned outcomes, the development and characterization of a novel nanocarrier system consisting of GCS and CD intended for transmucosal delivery of lipophilic drugs seemed of interest.

The role of a hydrophobic drug candidate is herein played by the fluorescent dye 6-coumarin (6-COUM), whose low loading requirement for nanoparticles (due to its high fluorescent activity) has already allowed to visualize brain uptake (Panyam and Labhasetwar, 2003a; Lu et al., 2005; Gao et al., 2007). However, the major drawback connected to the use of 6-COUM is that its solubility is negligible in water (2×10^{-8} M), but highly soluble in acetonitrile, ethanol, DMSO, DMF, chloroform or acetone and thus, it was well entrapped into hydrophobic matrices like poly(D,L-lactide-co-glycolide) nanoparticles (Panyam et al., 2003b). Due to the poor aqueous solubility of 6-COUM, through the inclusion of the fluorescent marker in the hydrophobic cavity of CD, we have reached its encapsulation in the hydrophilic network of GCS, probably because the host molecule (i.e., CD) exposes its external –OH groups to GCS. It should be noted that several coumarins were already reported to be accommodated into the hydrophobic cavities of CDs through non-covalent linkages and thanks to the external hydrophilic surface of the same CDs, improvements in solubility and stability in water were observed (Dondon and Fery-Forgues, 2001; Nowakowska et al., 2001).

For visualization purposes, newly designed GCS nanoparticles have been already employed to elucidate atherosclerotic lesion imaging on the damaged endothelium (Park et al., 2008). On the other hand, the high fluorescence activity of 6-COUM allows the

* Corresponding author. Tel.: +39 080 544 2804; fax: +39 80 544 2764.
E-mail address: atrapani@farmchim.uniba.it (A. Trapani).

0378-5173/$ – see front matter © 2009 Elsevier B.V. All rights reserved.
doi:10.1016/j.ijpharm.2009.03.041

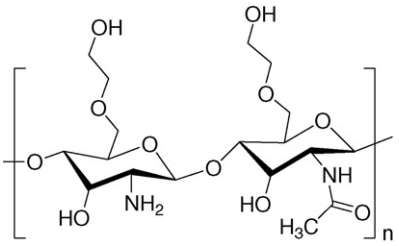

Fig. 1. The chemical structure of glycol chitosan (GCS).

replacement of hydrophobic drugs in the NPs formulations and the visualization and measurement of cellular uptake of the polymeric NPs, particularly because either the raw 6-COUM marker cannot be directly internalized by the cells or its leaking rate is low in the time scale of fluorescent observations (Win and Feng, 2005). To evaluate the potential of our GCS NPs as probes in biomedical field, the interaction of the particles was studied in the presence of human colorectal cancer cell line (Caco-2 cell line), a model cell line already reported in the literature for testing chitosan (Mao et al., 2005), and trimethylchitosan based drug carrier devices (Sandri et al., 2007). Importantly, to the best of our knowledge, no work has been carried out focusing on the interaction of GCS with Caco-2 and, thus far, the intracellular fate of GCS NPs has not been investigated, yet. Herein, Caco-2 cell monolayer was subjected to microscopic analysis by means of confocal laser scanning microscopy (CLSM) to highlight the interaction of the NPs with this biological substrate.

2. Materials and methods

Glycol chitosan (Mw = 68 kDa, from gel permeation chromatography; degree of acetylation = 10% and degree of glycol substitution = 62% from NMR spectroscopy), pentasodium tripolyphosphate (TPP), glycerol (99.5%, A.C.S.), polyvinyl alcohol (PVA, Mw = 49 kDa) and 6-coumarin were purchased from Sigma–Aldrich (Germany). Pluronic F68 (Mw = 8.4 kDa) was purchased from BASF (Ludwigshafen, Germany). Poly(lactic-co-glycolic) acid (PLGA) with a lactic to glycolic ratio of 50:50 (Resomer RG®504, Mw = 48 kDa) was purchased from Boehringer Ingelheim (Ingelheim, Germany). The natural beta-cyclodextrin (β-CD, Mw = 1135 Da) was provided by Schwartz Pharma, 2-hydroxypropyl-beta-cyclodextrin (HP-β-CD, Mw = 1431 Da, average substitution degree equal to 5) was purchased from Fluka, heptakis (2,6-di-O-methyl)-beta-cyclodextrin (DM-β-CD, Mw = 1131 Da, average substitution degree equal to 14) was purchased from Cyclolab. Gamma cyclodextrin (γ-CD, Mw = 1297 Da) and 2-hydroxypropyl-gamma-cyclodextrin (HP-γ-CD, Mw = 1576 Da, average substitution degree equal to 4) were provided by Wacker Chemie. Pure water (0.22 μm filtered, 0.055 S/cm, USF Seral, Seradest BETA 25) was used to prepare analytical solutions and buffers.

2.1. Fluorescence properties

Steady-state excitation and emission spectra were recorded at 25 °C on a fluorescent spectrophotometer (Safire II plate reader, Tecan AG, Mannedorf, Switzerland, excitation: 495 nm; emission 525 nm) in a conventional 96-well plate (Microtest™, Optilux™, Becton Dickinson, UK). The slit width was 5 nm for both excitation and emission and fluorescent top measurement mode was used throughout the study. All tested CDs were dissolved in water to give a final concentration of 2.5% (w/v) and care was taken to protect 6-COUM from natural and artificial light. Inclusion complexes between CD and 6-COUM were prepared at 1:1 molar ratio stoichiometry, by incubation of the two compounds in pure water under magnetic stirring for 24 h at room temperature. Then, the solutions were filtered (Millipore, pore size 0.45 μm) for analysis. The fluorescence spectra of pure 6-COUM in CH_3CN (2 mg/ml) and pure 6-COUM dispersed in water were taken as controls. The spectra were recorded without any correction for instrumental characteristics.

2.2. 6-COUM phase solubility studies

To assess the solubility of 6-COUM in the presence of DM-β-CD, Higuchi–Connors' method of phase solubility was employed. An excess amount of 6-COUM was added to 0, 0.009, 0.02, 0.04, 0.07, 0.08, 0.1, and 0.2 M solutions of DM-β-CD in double distilled water. The suspensions were kept in small tightly capped vials, agitated at 25 °C for 24 h, filtered (Millipore, pore size 0.45 μm) and fluorimetrically assayed for 6-COUM concentration. The linear range for fluorimetrically assay of 6-COUM was found over the range 1–370 ng/ml.

2.3. Nanoparticle preparation

2.3.1. Preparation of nanoparticles (GCS/TPP = 8.7/1, mass ratio)

NPs were prepared according to the mild ionic gelation technique as previously described by Trapani et al. (2008). Briefly, Pluronic F68 (0.2%, w/v) was added to 2.5 ml of the aqueous GCS solution (0.175%, w/v, pH about 5 before Pluronic F68 mixing). At room temperature and under stirring (250 rpm), the particles spontaneously formed upon addition of 0.5 ml of TPP aqueous solution (0.1%, w/v) to the above-mentioned GCS/Pluronic F68 solution.

2.3.1.1. 6-COUM loaded nanoparticles. 0.5 ml of the aqueous suspension 6-COUM (0.6%, w/v) were mixed with 0.25 ml of TPP aqueous solution (0.2%, w/v) to obtain an alkaline environment where the dye is chemically stable. Sonication of the mixture by Bandelin SONOREX RK 1028 squared apparatus (inner volume: 28l; inner space: 500 mm × 300 mm × 200 mm) was necessary to suspend the dye in the aqueous phase and the volumes in the mixture were adjusted in order to maintain GCS/TPP ratio equal to 8.7/1 (w/w). At room temperature, the particles spontaneously formed upon addition of this mixture to 2.5 ml of the aqueous solution containing GCS (0.175%, w/v) and Pluronic F68 (0.2%, w/v).

2.3.1.2. CD/6-COUM containing nanoparticles. The complexes 6-COUM: CD were prepared as reported in Section 2.1. For all CDs, 0.5 ml of complex solution were mixed with 0.25 ml of TPP aqueous solution (0.2%, w/v). NPs were spontaneously formed upon addition of the mixture complex/TPP to 2.5 ml of GCS (0.175%, w/v) previously dissolved in water in the presence of Pluronic F68 (0.2%, w/v).

2.3.2. Preparation of nanoparticles (GCS/TPP = 2.9/1, mass ratio)

NPs were prepared under stirring at room temperature at GCS/TPP ratio 2.9/1 (w/w) upon addition of 3 ml of TPP aqueous solution (0.07%, w/v) to 3 ml of GCS (0.2%, w/v) previously dissolved in acetic acid (1%, w/v) (Gan et al., 2005).

2.3.2.1. 6-COUM loaded nanoparticles. 0.5 ml of the suspension of 6-COUM in water (0.6%, w/v) was mixed with 1.50 ml of TPP aqueous solution (0.14%, w/v). NPs were spontaneously formed upon addition of this mixture to 3 ml of GCS (0.2%, w/v) previously dissolved in acetic acid (1%, w/v).

2.3.2.2. CD/6-COUM containing nanoparticles. For all CDs, 0.5 ml of complex solution was mixed with 1.5 ml of TPP aqueous solution (0.14%, w/v). NPs were spontaneously formed upon addition of the mixture complex/TPP to 3 ml of GCS (0.2%, w/v) previously dissolved in acetic acid (1%, w/v).

All formulated nanoparticles were isolated on a glycerol bed by ultracentrifugation (16,000 × *g*—60 min) and then resuspended in ultra pure water by manual shaking.

2.3.3. Preparation of PLGA nanoparticles

PLGA NPs were formulated as follows. 9.4 mg of DM-β-CD and 2.9 mg of 6-COUM were incubated in 12 ml of dichloromethane in Erlenmeyer flask under magnetic stirring for 24 h at room temperature to obtain a 1:1 molar ratio stoichiometry inclusion complex. After 24 h, 6.8 mg of PLGA were dissolved in 0.312 ml of the previously mentioned 6-COUM/DM-β-CD mixture and then emulsified in a 0.1% (w/v) solution of PVA prepared in ultra pure water. The formation of nanoparticles was allowed by using a microtip probe sonicator set at 50 W of energy outpout (Branson® Sonifier Cell Distruptor, Branson Ultrasonics Corporation, Garner, USA) for 30 s. Care was taken to correctly center the vessel of sampling with respect to the vertical tip. The removal of dichloromethane was carried out by evaporating for 2 h and, then, the pellets were collected by centrifugation at 14,000 × *g* for 30 min before incubation in the dissolution medium.

2.4. Physicochemical characterization of nanoparticles

For freshly prepared particles the mean particle size and the size distribution were determined in double distilled water by photon correlation spectroscopy (PCS) using Zetasizer NanoZS (ZEN 3600, Malvern, Herrenberg, Germany). The determination of the *ζ*-potential was performed using the technique of laser Doppler velocimetry using Zetasizer NanoZS after dilution with KCl 1 mM (pH 7.0). For zeta potential measurements, the refractivity index (RI) and viscosity of the KCl solution were used for calculations.

2.4.1. Determination of 6-COUM loading capacity and process yield

To determine 6-COUM NPs loading and process yield, batches of NPs were centrifuged (16,000 × *g*—60 min) and the pellet was then lyophilized for 48 h and weighted. To determine the 6-COUM content, a known amount of freeze-dried nanoparticles was analyzed using the following extraction protocol (Gao et al., 2007).

1 ml of ethyl acetate and 1 ml of water was added to freeze-dried nanoparticles, and then the particles were intensely vortexed for 5 min and the resulting mixture was centrifuged at 16,000 × *g* for 10 min. The supernatant was collected and evaporated under vacuum. The samples residues were reconstituted with 0.72 ml of acetonitrile and the fluorescent tracer concentrations were determined from a standard curve of 6-COUM in acetonitrile. The encapsulation efficiency and the process yield were calculated as follows:

$$\text{Encapsulation efficiency}\,(\%) = \frac{\text{actual loading}}{\text{theoretical loading}} \times 100$$

$$\text{Actual loading} = \frac{\text{weight of 6} - \text{COUM encapsulated in the NPs}}{\text{weight of NPs after freeze drying}}$$

$$\text{Theoretical loading} = \frac{\text{weight of 6} - \text{COUM initially added}}{\text{weight of total components}}$$

$$\text{Process yield}\,(\%) = \frac{\text{particles weight}}{\text{weight of total components}} \times 100$$

loading capacity and yield were the average of three batches.

2.4.2. Determination of CD content

The presence of CD in the pellet of GCS/TPP = 8.7/1 NPs containing 6-COUM/DM-β-CD was assessed by spectrophotometric analysis of the fading of phenolphthalein alkaline solutions (Da Silveira et al., 1998). Briefly, a 3 mM phenolphthalein stock solution in methanol was diluted 1:100 in 0.05 M carbonate buffer (pH 10.5). Freeze-dried NPs (obtained by freeze-drying 1 ml of NPs suspension) were dissolved in 1000 μl of water. 400 μl of this mixture were added to 2.6 ml of diluted phenolphthalein solution prepared as above described. The absorbance at 553 nm of resulting solution was measured by PerkinElmer Lamba Bio 20 spectrophotometer. For quantification, the DM-β-CD content was calculated by comparing the results to that of a standard curve obtained by using standard CD solutions. Linearity was checked in the range from 0.10 to 0.80 mg/ml).

2.5. Atomic force microscopy (AFM)

Atomic force microscopy was carried out to characterize the morphology of NPs. For AFM visualization, a drop of nanoparticle suspension was diluted in milliQ water (pH 5.5) and directly placed on a silicon chip. The observations were performed with a JPK NanoWizard (JPK Instruments, Berlin, Germany). The vibration-damped microscope was equipped with pyramidal Si3 N4 tips on a cantilever with a length of 125 μm, a resonance frequency of about 220 kHz and a nominal force constant of 36 N/m (NSC16 AlBs Micromasch, Estonia). To avoid damage of the sample surface all measurements were conducted in the intermittent contact mode. The scan speed was proportional to the scan size with a scan frequency from 0.5 to 1.0 Hz. Images were obtained by displaying amplitude, signal of the cantilever in the trace direction (Mao et al., 2006; Du et al., 2007).

2.6. In vitro release studies of 6-COUM containing NPs

In vitro release of 6-COUM from GCS NPs was performed to evaluate the amount of fluorescent tracer remained associated with the particles for 8 h.

6-COUM/DM-β-CD/glycol chitosan NPs (8.7/1, mass ratio) were collected by centrifugation, the pellets were resuspended and incubated in 1.2 ml of PBS (pH 7.4)/EtOH (99/1, v/v%) on a shaker at 37 °C under slow agitation. Ethanol was added to facilitate 6-COUM dissolution and fulfill the requirements of sink conditions. The amount of particles was adjusted to 1.2 mg/ml to obtain a maximum 6-COUM concentration in the range 80–350 ng/ml. Aliquots of 90 μl were then taken and replaced with fresh medium of equivalent volume (Gao et al., 2007). Each sample was subjected to centrifugation at 16,000 × *g* for 45 min. The pellet and the supernatant were collected, freeze-dried 48 h and analyzed for the released 6-COUM content as above described. The cumulative release percentage (CR%) of 6-COUM at each time point was calculated using the following equation:

$$\text{CR\%} = \frac{\text{amount of 6} - \text{COUM in the supernatant}}{\text{total amount of 6} - \text{COUM in the particles}} \times 100$$

PLGA NPs were also assayed for *in vitro* release test in PBS/EtOH medium as above reported for GCS NPs.

All experiments were carried out in triplicate. Standard deviation of measurements was ≤10%.

2.7. Cell uptake study

Caco-2 cells were used at passage 44–50 as described earlier (Walter and Kissel, 1995). Cells were seeded at a density of 6×10^4 cells/cm^2 on 6-wells uncoated polycarbonate Transwell™ filter inserts (Costar, Bodenheim, Germany, 0.4 μm pore size, area 4.71 cm^2) and cultivated over 21 days. The medium was changed every second day.

Cells were rinsed twice and equilibrated at 37 °C with pre-warmed uptake medium. The uptake medium was PBS supple-

mented with 25 mM glucose, 1.17 mM $CaCl_2$, 1.03 mM $MgCl_2$, pH 7.4. After the uptake medium was aspirated, the cells were incubated with 0.5 ml of 6-COUM/DM-β-CD glycol chitosan nanoparticle (8.7/1, mass ratio) suspension in uptake medium under different conditions. To investigate time-dependent uptake, cells were incubated for 5, 15, 30, 60, 120, 180 and 240 min at particle concentration of 0.25 mg/ml at 37 °C. 0.5 ml of the inclusion complex 6-COUM/DM-β-CD in uptake medium was taken as control. To investigate if energy-dependent endocytotic process could be responsible for NPs uptake, in one set of experiments, cells were incubated for 1 h at 4 °C with 0.5 ml of NPs at (0.062, 0.125, 0.25, 0.5, 1 mg/ml) in uptake medium. In a separate set of experiments, cells were incubated for 1 h at 37 °C with 0.5 ml of NPs at the same concentrations. After incubation, the test samples were aspirated; 0.1 ml of Trypan blue was post incubated with the cells for 1 min (0.4%, w/v in 0.1 M citrate buffer, pH 4.4) and, then, washed away. In fact, Trypan blue, by quenching the extracellular fluorescence, enables determination of the fraction of the particles which was actually internalized (Behrens et al., 2002).

The cells were washed three times with ice-cold transport buffer, fixated with 3.7% paraformaldehyde in PBS (pH 7.4) for 30 min at room temperature and counter-stained with the cell core marker TO-PRO-3 iodide (134.2 μg/l), for 20 min under light exclusion. Then, chambers were put off the slides and samples were embedded in gel/Mount™ (Biomeda, Italy), sealed with nail polish and imaged via CLSM (TCS SP2 Leica, Wetzlar, Germany) which was equipped with argon–krypton (488 nm) and helium–neon (633 nm) lasers. The fluorescence was monitored in the following channels: excitation 488 nm (for 6-COUM) and excitation 633 nm (for TO-PRO-3). Slides of untreated cells were used as negative control to determine microscope settings, which were maintained for all image capture and analysis. Confocal images were taken at 500 nm intervals on *z*-axis of the section. Images from individual optical planes and multiple serial optical sections were analyzed and the images were sequentially scanned on the two channels.

2.8. Statistics

Results are presented as means ± SD from at least three measurements. Significance between the mean values of size and zeta potential was calculated using ANOVA one-way analysis (GraphPad Prism v.4.00 GraphPad Software, Inc. San Diego, CA). Tukey tests were used for post hoc contrast. Differences from the controls (NPs without 6-COUM) were considered to be statistically significant at a level of $p \leq 0.05$ at 99% of confidence interval.

3. Results

3.1. Fluorescence properties

From the fluorescence excitation spectra it was evidenced a different behavior depending on the size of the cyclodextrin used thus, only the aqueous complexes of 6-COUM and β-CD, HP-β-CD and DM-β-CD showed an excitation maximum corresponding at 470 nm (Fig. 2A), whereas, at the same wavelength, either pure 6-COUM or γ-CD and HP-γ-CD were excited with weak fluorescence (Fig. 3A). Taking into account that at the wavelength of 508 nm the maximum emission for 6-COUM in acetonitrile occurs, when the solvent was replaced with water, the emission spectra for β-CDs complexes were blue shifted whereas the emission spectra for γ-CD and HP-γ-CD were red shifted, as already observed by Dondon and Fery-Forgues (2001) for the natural CDs.

In fact, by irradiating the test solutions at 470 nm, in the resulting emission spectra the observed maxima were found to depend

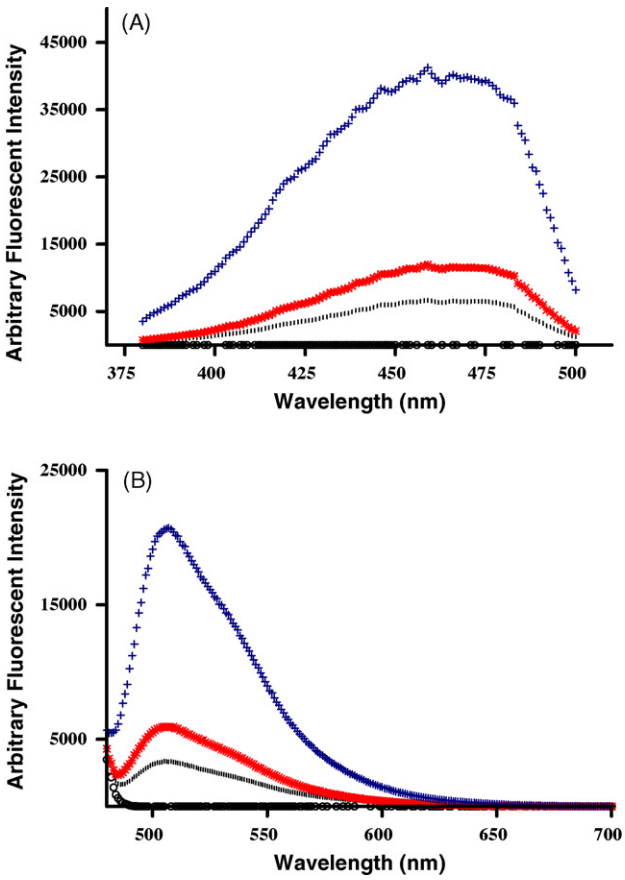

Fig. 2. The fluorescent intensity of 6-COUM/CD aqueous complexes as a function of the wavelength and the type of CD at 25 °C. (A) Excitation spectra from complexes of parent β-CD and its derivatives, HP-β-CD and DM-β-CD. (B) Emission spectra of the solutions of 6-COUM in the presence of β-CD, HP-β-CD and DM-β-CD. (◯) 6-COUM; (|) 6-COUM/β-CD; (*) 6-COUM/HP-β-CD; (+) 6-COUM/DM-β-CD.

on the type of ligand: 505 nm for β-CD, 506 nm for HP-β-CD and 507 nm for DM-β-CD (Fig. 3A), while the maxima at 554 and 547 nm for γ-CD and HP-γ-CD, respectively, appeared markedly quenched (Fig. 3B).

3.2. 6-COUM phase solubility studies

The aqueous solubility of 6-COUM was significantly enhanced upon addition of DM-β-CD, increasing from 2×10^{-8} M (in the absence of CD, i.e., intrinsic dye solubility) up to 8.82×10^{-3} M (when the concentration of DM-β-CD solution was set at 0.2 M), namely an enhancement of five magnitude orders was observed (Table 1). The plot of the data (Fig. 4) clearly showed a deviation of the curve from the linearity in a positive direction (A_P-type phase solubility diagram), suggesting the formation of higher order complexes. According to Higuchi and Connors (1965) treatment, the stability constants $K_{1:1}$ and $K_{1:2}$ of the complex were estimated by

Table 1
Solubility of 6-COUM in DM-β-CD solutions.

Concentration of CD[a] (M)	Solubility of 6-COUM (M)	Enhancement factor[b]
–	2.00×10^{-8}	–
0.02 (2.5%, w/v)	1.40×10^{-4}	5432
0.2 (25%, w/v)	8.82×10^{-3}	352,799

[a] Concentration of the aqueous cyclodextrin solution in water at 25 °C.
[b] The solubility of 6-COUM in the aqueous cyclodextrin solution divided by the solubility of 6-COUM in water.

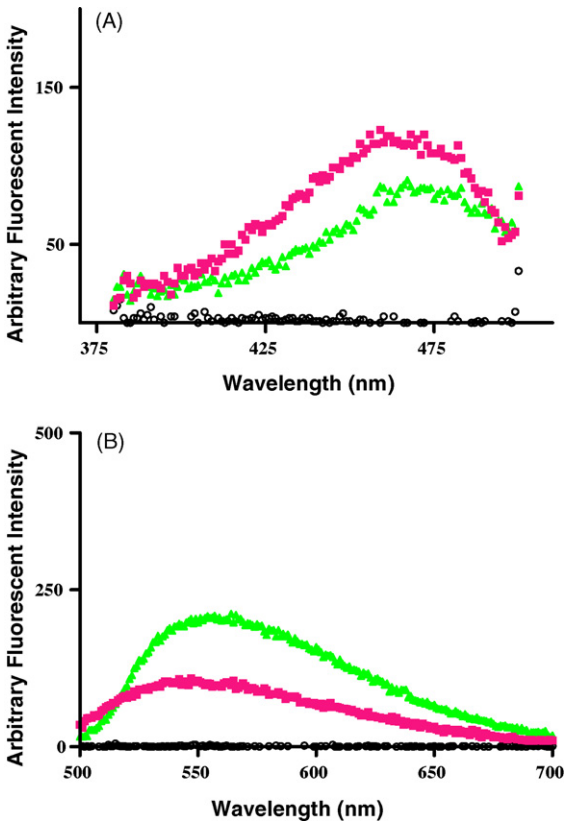

Fig. 3. (A). Excitation spectra from complexes containing γ-CD and HP-γ-CD. (B) Emission spectra of the solutions of 6-COUM in the presence of γ-CD and HP-γ-CD. (○) 6-COUM; (▲) 6-COUM/γ-CD; (□) 6-COUM/HP-γ-CD.

curve fitting with a quadratic model (Eq. (1)) (Loftsson et al., 2002)

$$S_t = S_0 + K_{1:1}S_0[\mathrm{CD}] + K_{1:1}\,K_{1:2}S_o[\mathrm{CD}]^2 \quad (1)$$

where [CD] is the molar concentration of DM-β-CD, S_o is the intercept of the curve, and $K_{1:2}$ is the apparent binding constant for higher order complexes. By manipulating the results from Fig. 4, the estimated $K_{1:1}$ value was 96.0 M^{-1} and $K_{1:2}$ value was 29.2 M^{-1}.

3.3. Physicochemical characterization of NPs:NPs (GCS/TPP = 8.7/1)

Physicochemical properties of the NPs under investigation are listed in Table 2 and Table 3. As suggested by Calvo et al. (1997) for chitosan NPs, GCS NPs were also prepared in the presence of Pluronic F68, yielding hydrodynamic diameters increased up to 350 nm (Table 2) because the surfactant increases the viscosity of the aqueous medium during particle formation. The role of Pluronic F68 is presumably "to delay" the ionic gelation process by locating itself at the interface air–liquid, with a consequent enlargement of the core of the nanosystem. Moreover, irrespective of the type of CD introduced, zeta potential of the particles was always close to +25 mV with the exception of NPs loaded with 6-COUM/γ-CD where zeta potential average was found equal to +19 mV. In this study, the theoretical loading for CD/GCS NPs was set equal to 3 10^{-5} wt.% and actual 6-COUM loading was found in the range 8×10^{-6} to 1×10^{-5} wt.%, with the most efficient formulation represented by DM-β-CD containing NPs and the least efficient formulation was the one containing only 6-COUM.

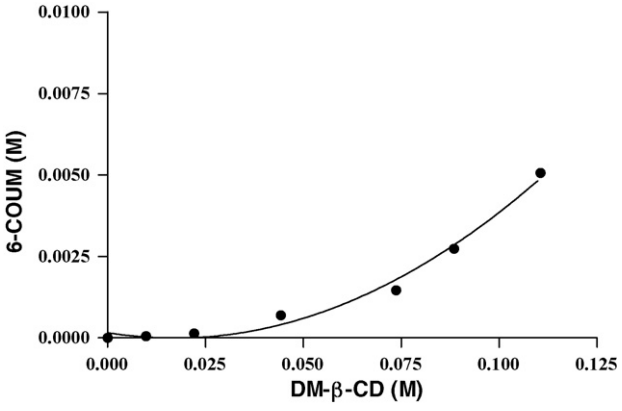

Fig. 4. Higuchi–Connors' plot of 6-COUM complexation with DM-β-CD after 24 h equilibrium at 25 °C.

3.4. Physicochemical characterization of NPs:NPs (GCS/TPP = 2.9/1)

When GCS and TPP were combined to give a mass ratio of 2.9/1 (Table 3), blue shade of the particles was optically seen and the photon correlation spectroscopy apparatus detected particles in the range 100–200 nm and polydispersity of 0.2. Furthermore, it resulted that the medium in which the polycation is dissolved affects the size of the resulting nanoparticles. In fact, when GCS was dissolved in acetic acid (1%, w/v), the pH measured was equal to 3.6 and the resulting particles were smaller than 200 nm. In the case of GCS/TPP NPs (8.7/1, mass ratio), the pH of the polycation aqueous solution was about 5 and, after the addition of Pluronic F68 (0.2%, w/v) a 0.2–0.4 pH unit increase was measured and, moreover, particle size was close to 300 nm.

For all formulations screened, encapsulation efficiency values of the particles GCS/TPP 2.9/1 were seen to be lower than that of the particles GCS/TPP 8.7/1. For 6-COUM/DM-β-CD loaded NPs at both GCS/TPP mass ratios, the encapsulation efficiency values were slightly higher than 30%.

3.5. Physicochemical characterization of PLGA NPs

For sake of comparison, poly(lactic-co-glycolic acid) (PLGA) nanoparticles loaded with 6-COUM were prepared and characterized *in vitro*. The molecular weight of PLGA used was similar to GCS and DM-β-CD was introduced in PLGA NPs which were 340 nm in size and displayed a 31% in encapsulation efficiency of 6-COUM.

3.6. Determination of CD content

For the quantitative analysis of CD content in particulate carriers, different approaches have been proposed in literature. The elemental analysis of freeze-dried particles is a convenient tool to determine the chemical composition of the particles by comparing the mass ratios of the pure components with the corresponding mass ratios in the particles (Trapani et al., 2008). In this work, we have studied the colorimetric reaction of phenolphthalein with the freeze-dried pellets of GCS/TPP = 8.7/1 NPs containing 6-COUM/DM-β-CD (Da Silveira et al., 1998). Reproducible amounts of 50% of the initial DM-β-CD content were associated with the DM-β-CD loaded NPs. In principles, 6-COUM could not interfere to the spectrophotometric assay at 553 nm because its UV spectrum showed no absorbance. Thus, when GCS/TPP = 8.7/1 NPs containing only 6-COUM underwent to the phenolphthalein test, no fading of phenolphthalein in the cuvette solutions occurred, indicating that the test was positive only if DM-β-CD was present in the NP matrix.

Table 2
Physicochemical properties of 6-COUM loaded NPs where GCS/TPP (8.7/1, mass ratio) (w/w) ($n = 3$).

NP formulation (w/w ratio)	Size (nm)	Polidispersiy	Zeta potential (mV)	Actual loading (wt.%)	Theoretical loading (wt.%)	Encapsulation efficiency (%)	Process yield (%)
GCS/TPP 8.7/1	348 (±24)	0.26 (±0.03)	+23.1 (±0.7)	0	0	0	13 (±1)
GCS/TPP 8.7/1 containing 6-COUM	299 (±25)	0.26 (±0.01)	+29.8* (±0.6)	8.8×10^{-6} ($\pm 2.0 \times 10^{-6}$)	8.0×10^{-5}	11.0 (±1.0)	18 (±1)
GCS/TPP 8.7/1 containing 6-COUM/β-CD	374 (±28)	0.36 (±0.03)	+25.0 (±2.0)	9.0×10^{-6} ($\pm 7.0 \times 10^{-7}$)	3.3×10^{-5}	27.0 (±2.0)	8 (±0)
GCS/TPP 8.7/1 containing 6-COUM/HP-β-CD	408 (±31)	0.29 (±0.09)	+25.9 (±1.3)	8.4×10^{-6} ($\pm 2.0 \times 10^{-6}$)	3.3×10^{-5}	25.4 (±1.0)	13 (±2)
GCS/TPP 8.7/1 containing 6-COUM/DM-β-CD	377 (±30)	0.32 (±0.06)	+25.2 (±2.0)	1.2×10^{-5} ($\pm 1.9 \times 10^{-6}$)	3.4×10^{-5}	35.0 (±3.0)	12 (±1)
GCS/TPP 8.7/1 containing 6-COUM/γ-CD	332 (±10)	0.25 (±0.02)	+19.7 (±1.9)	8.8×10^{-6} ($\pm 2.0 \times 10^{-6}$)	3.4×10^{-5}	26.0 (±3.0)	10 (±1)
GCS/TPP 8.7/1 containing 6-COUM/HP-γ-CD	328 (±28)	0.25 (±0.01)	+22.3 (±0.8)	7.7×10^{-6} ($\pm 1.0 \times 10^{-6}$)	3.4×10^{-5}	23.0 (±2.0)	8 (±1)

* $p < 0.001$.

Table 3
Physicochemical properties of GCS TPP NPs (2.9/1, mass ratio).

NP formulation (w/w ratio)	Size (nm)	Polidispersity	Zeta potential (mV)	Actual loading (wt.%)	Theoretical loading (wt.%)	Encapsulation efficiency (%)	Process yield (%)
GCS/TPP 2.9/1	128 (±39)	0.16 (±0.02)	+24.3 (±2.4)	0	0	0	43 (±4)
GCS/TPP 2.9/1 containing 6-COUM	195 (±9)	0.16 (±0.08)	+18.6* (±2.3)	4.3×10^{-6} ($\pm 6.0 \times 10^{-7}$)	1.4×10^{-4}	3.0 (±0.0)	22 (±1)
GCS/TPP 2.9/1 containing 6-COUM/β-CD	193 (±16)	0.26 (±0.04)	+18.8 (±0.8)	1.3×10^{-6} ($\pm 2.0 \times 10^{-7}$)	7.0×10^{-5}	2.0 (±0.0)	26 (±4)
GCS/TPP 2.9/1 containing 6-COUM/HP-β-CD	219* (±41)	0.24 (±0.03)	+17.6* (±1.6)	8.0×10^{-6} ($\pm 1.0 \times 10^{-6}$)	$5.0 \times ^{-5}$	16.0 (±1.0)	31 (±1)
GCS/TPP 2.9/1 containing 6-COUM/DM-β-CD	201 (±22)	0.23 (±0.02)	+19.1 (±1.9)	1.3×10^{-5} ($\pm 1.0 \times 10^{-6}$)	4.0×10^{-5}	33.0 (±3.0)	23 (±1)
GCS/TPP 2.9/1 containing 6-COUM/γ-CD	180 (±17)	0.22 (±0.03)	+19.3 (±2.7)	4.1×10^{-6} ($\pm 2.0 \times 10^{-7}$)	5.0×10^{-5}	8.0 (±0.0)	25 (±1)
GCS/TPP 2.9/1 containing 6-COUM/HP-γ-CD	170 (±31)	0.24 (±0.03)	+21.2 (±1.7)	3.0×10^{-6} ($\pm 2.0 \times 10^{-7}$)	5.0×10^{-5}	6.0 (±0.0)	23 (±1)

N.D.: not determined. ($n = 3$).
* $p < 0.05$.

3.7. AFM observations

AFM is a suitable technique to investigate the contribution of two parameters to the final morphology of the nanosystems, namely the method of particle preparation and the presence of DM-β-CD. Firstly, for each sample, the particle size measurements obtained by dynamic light scattering were in good agreement with size data determined by analysis of AFM images. As shown in (Fig. 5A and B), most of the particles were spherical with a smooth surface. In details, for 6-COUM/DM-β-CD GCS/TPP NPs 2.9/1 small particles were detected inside larger structures and, moreover, when the conditions of particles preparation were adjusted to achieve GCS/TPP NPs 8.7/1, (Fig. 5C and D), an excess of GCS polymer outside of NP was observed. This finding could be explained in terms of the process yield of GCS/TPP NPs 8.7/1 lower than GCS/TPP NPs 2.9/1. Accordingly, GCS polymer which was not involved in NP formation was visualized in the form of aggregates, similarly to the images of unreacted chitosan chains as reported by Mao et al. (2006). Thus, in the tested formulations the particle preparation method rather than the presence or the absence of DM-β-CD affects in some extent the morphology.

3.8. In vitro release studies

In view of the application of 6-COUM NPs as novel probes for cellular tracking, the release of 6-COUM from 6-COUM/DM-β-CD GCS NPs was carried out in PBS at 37 °C and the results are shown in Fig. 6. The choice of these particles was due to their greater encapsulation efficiency. Moreover, the study was performed up to 8 h taking into account that cell viability is no longer than 5 h. For the sake of comparison, we have also evaluated the release of 6-COUM from PLGA NPs containing the same CD. For both type of particles, 6-COUM was released from NPs following a biphasic pattern: a rapid initial release that occurred in few min followed by a slow release. After 1 h, the burst effect for GCS NPs was found higher than the corresponding one from PLGA NPs (i.e., 14 and 1% of the tracer, respectively).

3.9. Confocal microscopy in Caco-2 cell line

DM-β-CD/GCS NPs (8.7/1) (i.e., the NPs characterized by the highest encapsulation efficiency) were selected for cell uptake studies. The incubation time of particles was set to 4 h in order

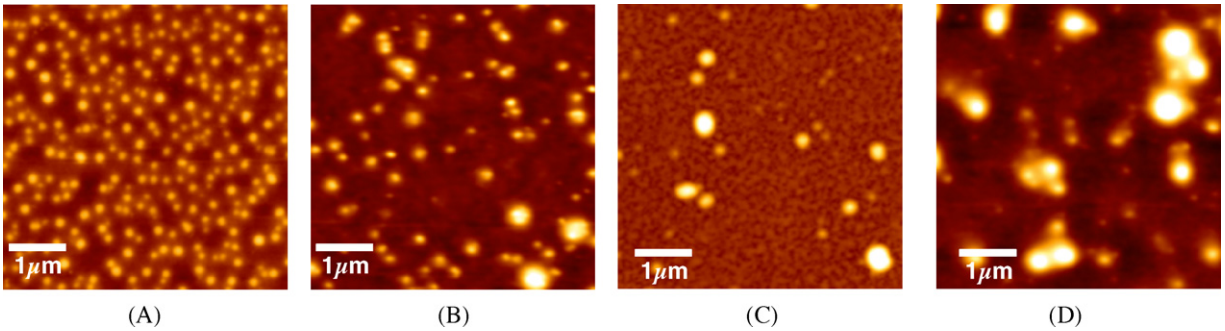

Fig. 5. Atomic force microscopy images of selected 6-COUM NPs. (A) GCS/TPP NPs containing only 6-COUM (2.9/1) [average size by AFM = 202 (±33) nm]; (B) 6-COUM/DM-β-CD loaded GCS/TPP NPs (2.9/1) [average size by AFM = 230 (±30) nm]; (C) GCS/TPP NPs containing only 6-COUM (8.7/1) [average size by AFM = 326 (±62) nm]; (D) 6-COUM/DM-β-CD loaded GCS/TPP NPs (8.7/1) [average size by AFM = 368 (±65) nm].

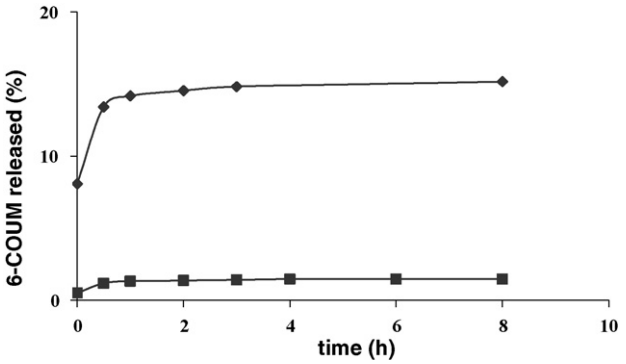

Fig. 6. *In vitro* release profiles of 6-COUM in PBS (pH 7.4)/EtOH (99/1, v/v%) from GCS NPs (♦) and PLGA NPs (■).

to minimize the risk to detect the free dye by fluorescent microscopy.

For confocal microphotographs, TO-PRO-3 was used as a marker for cell nuclei of Caco-2 cells giving a typical blue fluorescence (Loverre et al., 2004) and to distinguish between membrane-associated and internalized complexes, Trypan blue was employed throughout the study. It is well known that viable cells excluded Trypan blue molecules; consequently, the residual fluorescence implied the existence of a substantial amount of intracellular NPs, rather than cell surface adsorption. As shown in Fig. 7A–C, the internalization of the particles in Caco-2 cells is a time-dependent process. Up to 15 min of incubation at 37 °C, the particles were detected in the extracellular medium and no internalization occurred. Starting from 30 min, GCS NPs were transferred into the cytoplasm and, the uptake increased up to 4 h when the fluorescent carriers were detected in the perinuclear region (Fig. 7C) as already seen in the case of trimethylchitosan-insulin nanocomplexes (Mao et al., 2005). According to the previous results, when the concentration of the particles was equal to 1 mg/ml at 37 °C (Fig. 7D), 1 h of incubation was found to be a suitable time to achieve the localization close to the cell nuclei.

To investigate if energy-dependent endocytotic process could be responsible for NPs uptake, the incubation of the particles was also performed at 4 °C because the low temperature is known to block active transport processes. Surprisingly, at rather high particle concentrations (0.25 and 1 mg/ml) at 4 °C, the green fluorescence was

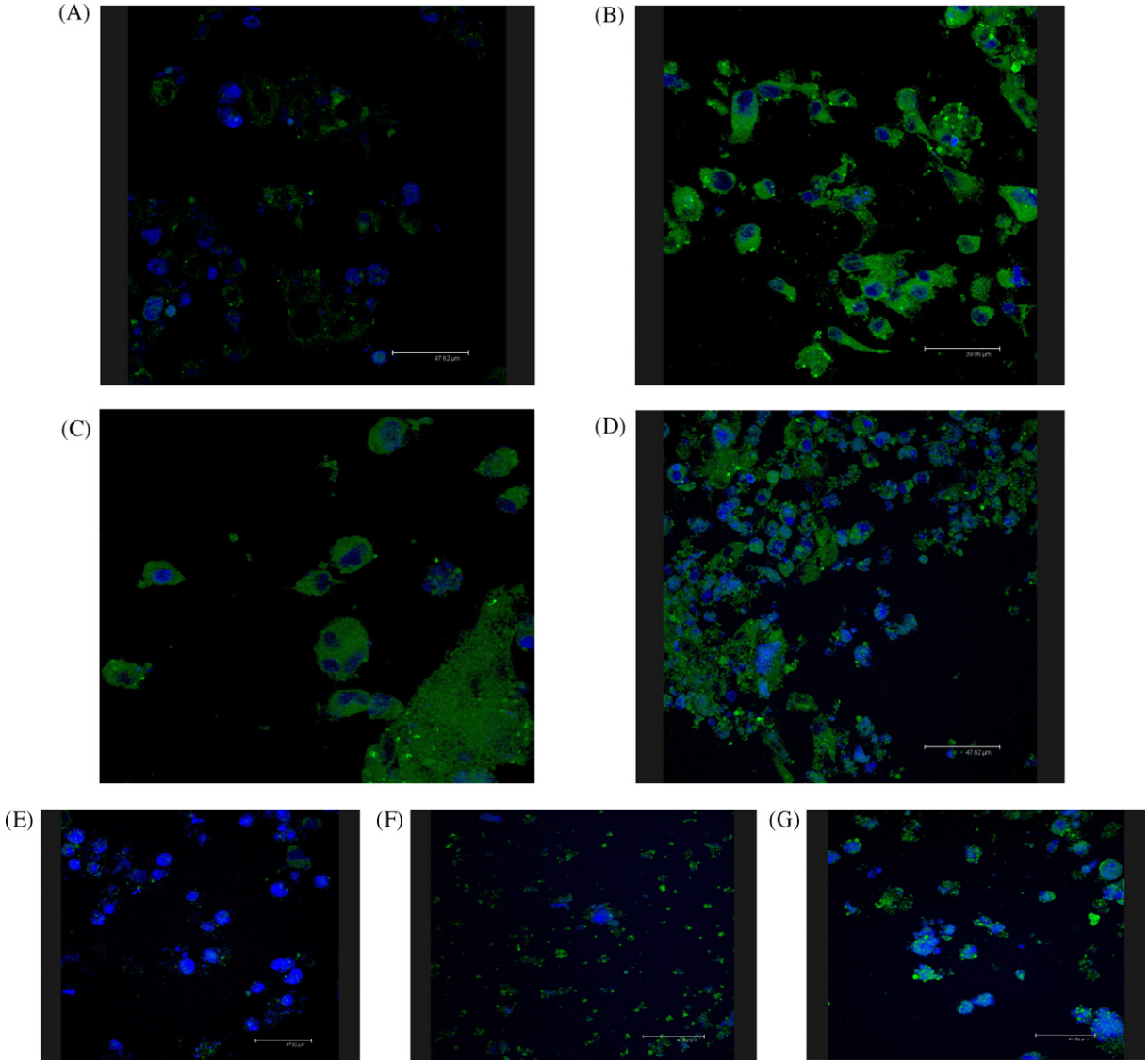

Fig. 7. Confocal micrograph images of Caco-2 cell monolayers incubated with 6-COUM/DM-β-CD GCS NPs upon different conditions. (A) Particle concentration: 0.25 mg/ml—incubation: 5 min at 37 °C; (B) particle concentration: 0.25 mg/ml—incubation: 2 h at 37 °C; (C) particle concentration: 0.25 mg/ml—incubation: 4 h at 37 °C; (D) particle concentration: 1.0 mg/ml—incubation: 1 h at 37 °C; (E) particle concentration: 0.062 mg/ml—incubation: 1 h at 4 °C; (F) particle concentration: 0.25 mg/m—incubation: 1 h at 4 °C; (G) particle concentration: 1.0 mg/ml—incubation: 1 h at 4 °C.

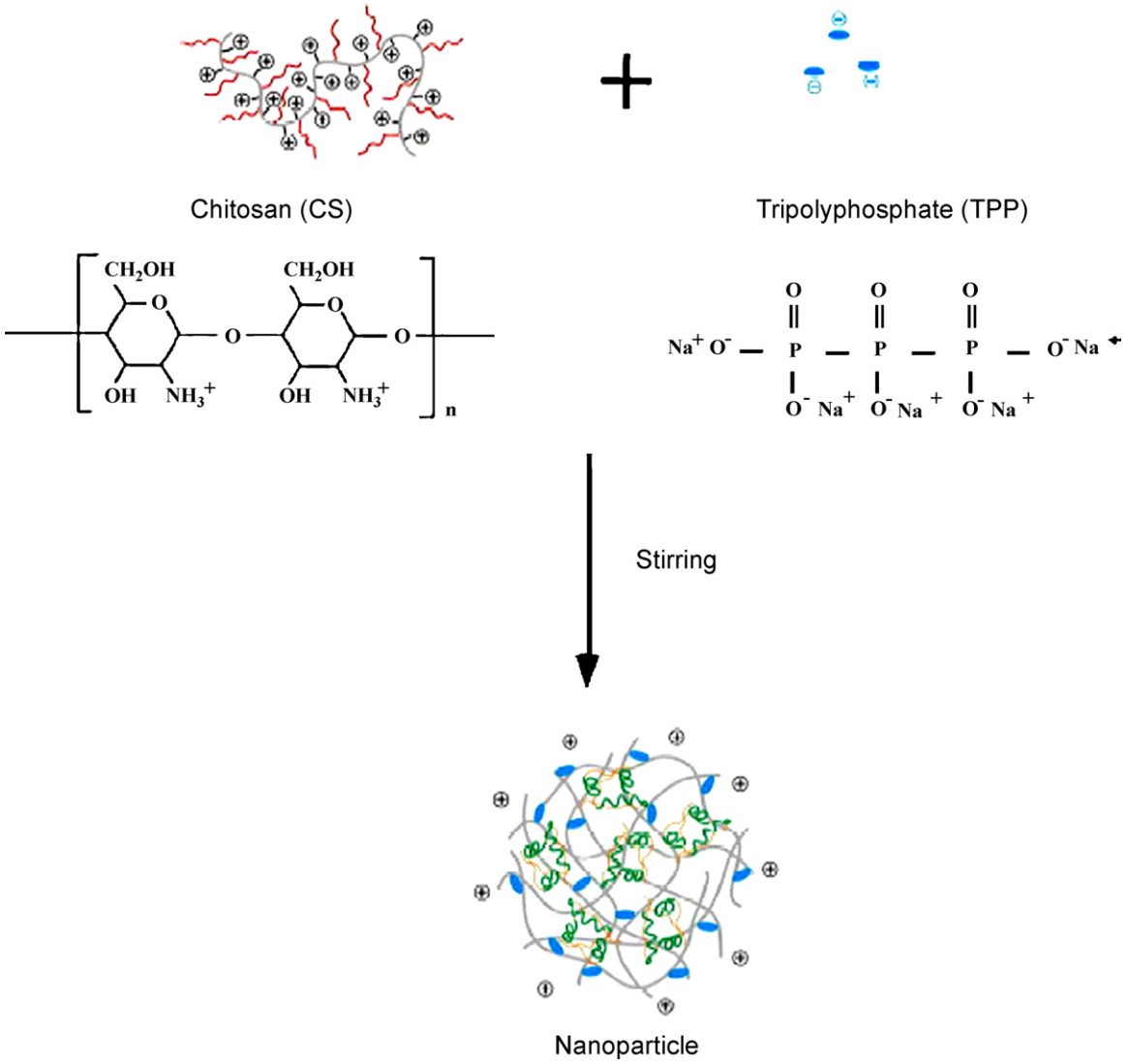

Fig. 8. Schematically formulation of GCS/TPP NPs.

localized in the cytoplasm of Caco-2 cells (Fig. 7F and G, respectively) whereas no *locus* of green fluorescence could be revealed for lower concentration like 0.062 mg/ml (Fig. 7E). It was consistent with the fact that the low temperature only slowed down the transport of the particles but did not inhibit it.

4. Discussion

The aim of the present study was to develop and characterize GCS NPs that would be suitable for the encapsulation of the poor water soluble 6-COUM in the presence of CD and evaluate by confocal microscopy the intracellular fate of these systems. Herein, we worked with a low-Mw chitosan derivative according to the fact that low-Mw chitosan can be potentially useful as parenteral drug carriers due to a lower antigen effect and nephrotoxicity (Richardson et al., 1999). In this regard, however, it should be considered that chitosans of parenteral grade are a very expensive raw materials and, due to the fact that they are derived from a natural source, are subject to variability in quality. Low water soluble drugs can be easily accommodated inside the cavity of CDs by forming *host–guest* inclusion complexes, with consequent benefits including increase in solubility and in bioavailability. Based on the findings by Maestrelli et al. (2006), we hypothesized that 6-COUM acts as a model hydrophobic guest capable to be accommodated in the cavity of CD, whereas the external –OH groups of the CD can conveniently interact with the hydrophilic network of GCS via hydrogen bonding and non-covalent linkages. From this background, the first step of the work focused on the interaction of 6-COUM and CDs in water medium by exploring fluorescence spectra of the resulting complexes. The enhanced fluorescence intensity for both excitation and emission gives a strong indication of the inclusion complex formation (Takakusa et al., 2001) and it can be explained in terms of the decrease of the intramolecular rotational freedom of the dye molecule in the restricted microenvironment of the oligosaccharide (Ma et al., 2000).

It is well known that dyes undergo processes such as aggregation and photo oxidation which influence the efficiency of emission (Nowakowska et al., 2001). The products formed in these reactions can absorb the laser light or quench the molecules of coumarin in their excited singlet states thus decreasing the efficiency of emission. γ-CD was demonstrated to reduce the photo bleaching of 151-COUM and 120-COUM (Yamagouchi and Higashi, 1990); on the other hand, Sen et al. (2005) demonstrated that 153-COUM was included almost at 66% into the cavity of DM-β-CD, leading to a marked increase of the aqueous solubility of the dye.

Our fluorescence analysis showed that DM-β-CD provides a hydrophobic host cavity for the dye under better conditions than the other tested CDs (especially for large cycles like γ-CDs possessing eight sugar units forming the cavity) and, therefore, we performed phase solubility studies of 6-COUM by increasing the concentrations of DM-β-CD. The literature value for the association constant for 153-COUM and DM-β-CD is 220 M^{-1}, a higher value than that for 6-COUM (96.0 M^{-1}) which is not surprising considering the differences in the chemical structures of these compounds. Overall, the apparent binding constant value is related to the reciprocal interaction between the oligosaccharide and the dye and this interaction could be of aid to encapsulate the hydrophobic 6-COUM in the hydrophilic matrix of GCS. In fact, as indicated by the enhancement factors reported in Table 1, DM-β-CD exhibits a greater solubilizing power for 6-COUM and the complexation was expected to provide a higher entrapment in the GCS nanocarriers.

In principle, GCS NPs were designed in the size range 200–300 nm to allow cell internalization process according to endocytosis pathway. For this purpose, the ionic gelation technique (Gan et al., 2005) was adopted to formulate the novel nanosystems because the convenience of such approach mainly relies on the simple mixing of oppositely charged aqueous solutions without any organic solvent or covalent cross-linking agent (i.e., gluteraldehyde) as depicted in Fig. 8.

The high solubilizing capability of DM-β-CD for 6-COUM may explain the high loading of the corresponding particles (GCS/TPP = 8.7/1) whereas for HP-γ-CD-based NPs presumably either the larger cavity of the CD or the effect of the substituents could be involved in the low drug loading. These findings confirm our hypothesis that the introduction of CDs could help to load the hydrophobic 6-COUM in the hydrophilic matrix of GCS because when no CD was employed, encapsulation efficiency went down to 11 and 3% for GCS/TPP = 8.7/1 and GCS/TPP = 2.9/1 particles, respectively. In this work, the NP formulation candidate for cell studies (i.e., 6-COUM/DM-β-CD GCS/TPP = 8.7/1) was taken as model for the colorimetric reaction with phenolphthalein for the assessment of the CD. This test demonstrated that the oligosaccharide was still present in the pellets of NPs and, consequently, the same DM-β-CD is able to force 6-COUM to be entrapped in the GCS network.

About NPs characterization, GCS/TPP 2.9/1 NPs, showing a polyction/polyanion mass ratio lower than GCS/TPP 8.7/1 ones, exhibit zeta values in the range +17 to +20 mV whereas the latter gave zeta potentials close to +25 mV. This finding is in good agreement with the simple linear relationship already seen with chitosan by Gan et al. (2005). The authors found that the zeta potential of chitosan/TPP NPs increased linearly with increasing chitosan to TPP weight from 3/1 to 7/1 for high, medium and low molecular weight chitosan. This feature represents for us an interesting way to modulate the particle surface charge density and, thus, to facilitate the adhesion and transport properties of the NPs. Additionally, GCS/TPP = 2.9/1 NPs provided process yields bigger than 20%, in good agreement with Janes and Alonso (2003) who found process yields in the range 26–36% for CS/TPP NPs 3/1 and chitosan in the range of molecular weight 38–70 kDa. On the other hand, for NPs GCS/TPP = 8.7/1 yield values were in the range 10–20% with the exception of NPs containing β-CD and HP-γ-CD. β-CD is the lowest water soluble oligosaccharide and, due to the fact that the ionic gelation technique takes place in aqueous medium, it is possible that such CD partially contributes to the final yield of production. Generally, for our particles, we agree with the explanation by Fernandez-Urrusuno et al. (1999) who stated that the yield is related to the particle formation mechanism. NPs are mainly formed by interaction between GCS and the counter ion TPP and, therefore, the incorporation of increasing amounts of TPP (as for GCS/TPP 2.9/1) leads to the formation of a greater number of particles. In the present work, we have shown that by simple modifications of the ionic gelation technique, particles bigger than 300 nm and particles smaller than 250 nm were achieved (Tables 2 and 3).

Prior to cell uptake observations, *in vitro* 6-COUM release from GCS and PLGA NPs was studied in PBS at 37 °C. As shown in Fig. 6, 6-COUM is released in greater amount from GCS NPs than the PLGA based containing the same CD and used as control. Taking into account that GCS and PLGA NPs were similar in size and 6-COUM content, according to Mu and Feng (2003) the different release profile should be due to an internal structure more compact for PLGA NPs, hindering the water penetration into the particles and, hence, there is less drug diffusion towards the release medium. It seems that the amount of 6-COUM on the GCS particle surface is released in the form of a burst, while the tracer incorporated within the particle core is released over a more prolonged period.

From the results of cell uptake studies (Fig. 7), for the first time the occurrence of adsorptive transcytosis of GCS based NPs across Caco-2 cells was confirmed by CLSM, similarly to the mechanism observed for mucoadhesive chitosan based NPs (Behrens et al., 2002) and chitosan coated NPs (Kim et al., 2008).

In conclusion, in the present work we describe the feasibility of employing the ionic gelation technique to formulate GCS based NPs where the loading of a hydrophobic molecule such as 6-COUM was allowed by the introduction of cyclodextrins. Although 6-COUM was more strictly retained in PLGA NPs than GCS NPs, the latter were prepared in the absence of any organic solvent in aqueous medium resulting in higher biocompatibility. From the incubation with Caco-2 cells line, 6-COUM containing GCS NPs seem to be promising for studying intracellular NPs uptake and distribution using confocal microscopy. Further studies will be addressed to understand the contributions of paracellular and transcellular pathways to the whole NPs internalization process, maximizing the effective delivery of the particles into the cells.

Acknowledgments

Adriana Trapani would like to acknowledge the German Academic Exchange Service (Deutsche Akademische Austauschdienst, DAAD) for the financial support. We thank Christian Hobler (Philipps Universität, Marburg, Germany) for his helpful discussion with fluorescence analysis and Dr. Antonella Loverre (Dipartimento di Emergenza Trapianti di Organi, (D.E.T.O) Bari Hospital, Bari, Italy) for interpretation of confocal microphotographs.

References

Behrens, I., Vila Pena, A.I., Alonso, M.J., Kissel, T., 2002. Comparative uptake studies of bioadhesive and non-bioadhesive nanoparticles in human intestinal cell lines and rats: the effect of mucus on particle uptake adsorption and transport. Pharm. Res. 19, 1185–1193.

Calvo, P., Remunan-Lopez, C., Vila-Jato, J.L., Alonso, M.J., 1997. Novel hydrophilic chitosan polyethylene oxide nanoparticles as protein carriers. J. Appl. Polym. Sci. 63, 125–132.

Da Silveira, A.M., Ponchel, G., Puisieux, F., Duchene, D., 1998. Combined poly(isobutylcyanoacrilate) and cyclodextrins nanoparticles for enhancing the encapsulation of lipophilic drugs. Pharm. Res. 15, 1051–1055.

Dondon, R., Fery-Forgues, S., 2001. Inclusion complex of fluorescent 4-hydroxycoumarin derivatives with native β-cyclodextrin: enhanced stabilization induced by the appended substituent. J. Phys. Chem. 105, 10715–10722.

Du, Y., Luo, X.-L., Xu, J.-J., Chen, H.-J., 2007. A simple method to fabricate a chitosan gold nanoparticles film and its application in glucose biosensor. Bioelectrochemistry 70, 342–347.

Fernandez-Urrusuno, R., Romani, D., Calvo, P., Vila-Jato, J.L., Alonso, M.J., 1999. Development of freeze-dried formulation of insulin loaded chitosan nanoparticles intended for nasal administration. STP Pharma Sci. 9, 429–436.

Gan, Q., Wang, T., Cochrane, C., McCarron, P., 2005. Modulation of surface charge, particle size and morphological properties of chitosan–TPP nanoparticles intended for gene delivery. Colloids Surf. B: Biointerfaces 44, 65–73.

Gao, X., Chen, J., Tao, W., Zhu, J., Zhang, Q., Chen, H., Jiang, X., 2007. UEA I-bearing nanoparticles for brain delivery following intranasal administration. Int. J. Pharm. 340, 207–215.
Higuchi, T., Connors, K.A., 1965. Phase-solubility techniques. Adv. Anal. Chem. Instrum. 4, 117–212.
Janes, K.A., Alonso, M.J., 2003. Depolymerized chitosan nanoparticles for protein delivery: preparation and characterization. J. Appl. Polym. Sci. 88, 2769–2776.
Kim, B.-S., Kim, C.-S., Lee, K.-M., 2008. The intracellular uptake ability of chitosan coated poly(D,L-lactide-co-glycolide) nanoparticles. Arch. Pharm. Res. 31, 1050–1054.
Krauland, A.H., Alonso, M.J., 2007. Chitosan/cyclodextrin nanoparticles as macromolecular drug delivery system. Int. J. Pharm. 340, 134–142.
Loftsson, T., Magnusdottir, A., Masson, M., Sigurjonsdottir, J., 2002. Self association and cyclodextrin solubilization of drugs. J. Pharm. Sci. 91, 2307–20316.
Loverre, A., Ditonno, P., Crovace, A., Gesualdo, L., Ranieri, E., Pontrelli, P., Stallone, G., Infante, B., Schena, A., Di Paolo, S., Capobianco, C., Ursi, M., Palazzo, S., Battaglia, M., Selvaggi, F.P., Schena, F.P., Grandaliano, G., 2004. Ischemia-reperfusion induces glomerular and tubular activation of proinflammatory and antiapoptotic pathways: differential modulation by rapamycin. J. Am. Soc. Nephrol. 15, 2675–2686.
Lu, Y., Zhang, Y., Tan, Y.-Z., Hu, K.-L., Jiang, X.-G., Fu, S.-K., 2005. Cationic albumin-conjugated pegylated nanoparticles as novel drug carrier for brain delivery. J. Control. Release 107, 428–448.
Ma, D.Q., Rajewski, R., Vander Velde, D., Stella, V.J., 2000. Comparative effects of $(SBE)_{7m}$-β-CD and HP-β-CD on the stability of two antineoplastic agents, melphalan and carmustine. J. Pharm. Sci. 89, 275–286.
Maestrelli, F., Garcia-Fuentes, M., Mura, P., Alonso, M.J., 2006. A new drug nanocarrier system consisting of chitosan and hydroxypropylcyclodextrin. Eur. J. Pharm. Biopharm. 63, 79–86.
Mao, S., Bakowsky, U., Jintapattanakit, A., Kissel, T., 2006. Self assembled polyelectrolyte nanocomplexes between chitosan derivatives and insulin. J. Pharm. Sci. 95, 1035–1048.
Mao, S., Germershaus, O., Fischer, D., Linn, T., Schnepf, R., Kissel, T., 2005. Uptake and transport of PEG-graft-trimethyl-chitosan copolymer-insulin nanocomplexes by epithelial cells. Pharm. Res. 22, 2058–2068.
Mei, D., Mao, S., Sun, W., Wang, Y., Kissel, T., 2008. Effect of chitosan structure properties and molecular weight on the intranasal absorption of tetramethylpyrazine phosphate in rats. Eur. J. Pharm. Biopharm. 70, 874–881.
Mu, L., Feng, S.-S., 2003. PLGA/TPGS nanoparticles for controlled release of paclitaxel: effects of emulsifier and drug loading ratio. Pharm. Res. 20, 1864–1872.
Nowakowska, M., Smoluch, M., Sendor, D., 2001. The effect of cyclodextrins on the photochemical stability of 7-amino 4-methyl coumarin in aqueous solution. J. Inclus. Phenom. 40, 213–219.
Panyam, J., Labhasetwar, V., 2003a. Dynamics of endocytosis and esocytosis of poly(D,L-lactide-co-glycolide) nanoparticles in vascular smooth muscle cells. Pharm. Res. 20, 212–220.
Panyam, J., Sahoo, S.K., Prabha, S., Bargar, T., Labhasetwar, V., 2003b. Fluorescence and electron microscopy probes for cellular and tissue uptake of poly(D,L-lactide-co-glycolide) nanoparticles. Int. J. Pharm. 262, 1–11.
Park, K., Hong, H.-Y., Moon, H.J., Lee, B.-H., Kim, I.-S., Kwon, I.C., et al., 2008. A new atherosclerotic lesion probe based on hydrophobically modified chitosan nanoparticles functionalized by the atherosclerotic plaque targeted peptides. J. Control. Release 128, 217–223.
Richardson, S.C.W., Kolbe, H.V.J., Duncan, R., 1999. Potential of low molecular mass chitosan as a DNA delivery system: biocompatibility, body distribution and ability to complex and protect DNA. Int. J. Pharm. 178, 231–243.
Sandri, G., Bonferoni, M.C., Rossi, S., Ferrari, F., Gibin, S., Zambito, Y., Di Colo, G., Caramella, C., 2007. Nanoparticles based on N-trimethylchitosan: evaluation of absorption properties using *in vitro* (Caco-2 cells) and *ex vivo* (excised rat jejunum) models. Eur. J. Pharm. Biopharm. 65, 68–77.
Sen, P., Roy, D., Mondal, S.K., Sahu, K., Ghosh, S., Bhattacharyya, K., 2005. Fluorescence anisotropy decay and solvation dynamics in a nanocavity: coumarin 153 in methyl beta cyclodextrins. J. Phys. Chem. 109, 9716–9721.
Takakusa, H., Kikuchi, K., Urano, Y., Higuchi, T., Nagano, T., 2001. Intramolecular fluorescence resonance energy transfer system with coumarin donor included in β-cyclodextrin. Anal. Chem. 73, 939–942.
Trapani, A., Garcia-Fuentes, M., Alonso, M.J., 2008. A new drug nanocarrier combining hydrophilic cyclodextrins and chitosan. Nanotechnology 19, 185101/1–1185101/.
Walter, E., Kissel, T., 1995. Heterogeneity in the human intestinal cell line Caco-2 leads to differences in transepithelial transport. Eur. J. Pharm. Sci. 3, 215–230.
Win, K.Y., Feng, S.-S., 2005. Effects of particle size and surface coating on cellular uptake of polymeric nanoparticles for oral delivery of anticancer drugs. Biomaterials 26, 2713–2722.
Yamagouchi, H., Higashi, M., 1990. Inclusion effects of cyclodextrins on the photobleaching of coumarins. J. Inclusion. Phenom. 9, 51–54.